(Distribution Restricted)
until April 3, 1986

Crustal Structure of the Northwestern Gulf of Mexico, Offshore Texas: An Ocean-Bottom Seismograph - Air Gun Experiment

by

Yosio Nakamura, F. Jeanne Shaub,
Kevin MacKenzie and Jürgen Oberst

Final Report of Research Agreement

Submitted to Sponsor

November 30, 1985

Institute for Geophysics
The University of Texas at Austin
4920 North I.H. 35
Austin, Texas 78751

University of Texas Institute for Geophysics Technical Report No. 39

SUMMARY

We have conducted a large-offset seismic experiment in the northwestern Gulf of Mexico, offshore of Texas, using large-capacity air guns and ocean-bottom seismographs. The purpose of the experiment was to map the deep sedimentary and crustal structures underlying the thick sedimentary cover which also included many salt intrusives. Five lines, each approximately 90 km long with four or more OBS's, were shot over an area which extended from mid-shelf at about 70 m water depth to the continental rise just beyond the western end of the Sigsbee Escarpment at about 3000 m water depth.

The acquired data were analyzed and interpreted initially using standard techniques assuming the structure to be one dimensional: layer solutions from phase velocities and intercept times of refracted arrivals, continuous velocity profiles through direct inversion of first-arrival times, and interval velocities from moveout of wide-angle reflections. These velocity profiles are used as a guide to build a two-dimensional structural model of each line based on multichannel reflection data and various other arrivals, such as reflections from and refractions through salt intrusives, as observed on OBS seismic data. We then used two-dimensional ray tracing to match the theoretical arrivals with observed ones, refining both shallow structures as well as the depths to the deeper refractors.

The entire study area is covered with thick sediments, whose thickness varies from 13 to 15 km under the shelf and slope but thins to about 11 km under the continental rise. Among the several seismic reflectors found within the sedimentary column, the most prominent is the one which we interpret to be the middle Cretaceous unconformity (MCU) at a depth of 7 to 11 km. The seismic velocity in the sediment column above the MCU increases from 1.7-1.9 km/s near the sea floor to 3.0-4.0 km/s just above the MCU, representing mostly clastics. Below the MCU, the velocity increases to 3.7-4.7 km/s, suggesting carbonate or possibly salt. Many salt features are found within the sedimentary column.

The basement, or the top of the crust, as inferred from higher velocity refracted arrivals, is found at a depth of 13 to 16 km. The observed basement relief is quite consistent from line to line and shows a NW-SE trending ridge that may constitute a seaward extension of the San Marcos arch, and a trough that runs south of the ridge. The basement velocity is 5.0-5.2 km/s in the northern half of the study area, but increases to 5.6-5.8 km/s in the southern half of the area except for the southeastern corner, under the continental rise, where it increases further to 6.4 km/s. This velocity variation may represent a transition from purely continental through transitional to oceanic crust. The Moho is observed only at the southeastern corner of the study area, where it is at a depth of about 20 km under the continental rise and deepens somewhat towards the slope. Elsewhere, it appears to be deeper than 25 km.

INTRODUCTION

Wide areas of the northern Gulf of Mexico are underlain by thick sediments transported from the vast expanse of the North American continent since Late Jurassic time. Because of this thick sedimentary cover and also of numerous salt deposits that are found in many areas of this region, it is difficult, and often impossible, to probe the underlying crustal layers using seismic reflection techniques commonly used in the petroleum industry.

In order to acquire seismic data relevant to the deep crustal structure of the northern Gulf of Mexico, we have been conducting a series of large-offset seismic experiments using ocean-bottom seismographs (OBS) and large-capacity air-gun sources. The use of OBS,s allows us to extend seismic lines to very large offsets, thus enabling us to obtain refracted and wide-angle reflected arrivals from deep layers. The relative quiescence of the ocean floor compared with the sea surface is also advantageous for detection of weak seismic signals. Air guns provide more accurately timed, uniform and spatially denser source signals than conventional explosive sources commonly used in similar seismic refraction surveys.

This report covers the results of the third such experiment in the northern Gulf of Mexico. The earlier experiments covered an area offshore of eastern Texas coast (a report in preparation) and the Green Canyon area off the Louisiana coast[1]. The present experiment was carried out in early 1984 in the northwestern part of the Gulf off the southern Texas coast, Fig. 1.

---

[1]Y. Nakamura, D. S. Sawyer, J. O. Ebeniro, W. P. O'Brien, Jr., F. Jeanne Shaub and J. Oberst, "Crustal Structure of the Green Canyon Area, Northern Gulf of Mexico: An Ocean-Bottom Seismograph - Air Gun Experiment", Tech. Rept. No. 38, University of Texas Institute for Geophysics, Austin, 1985.

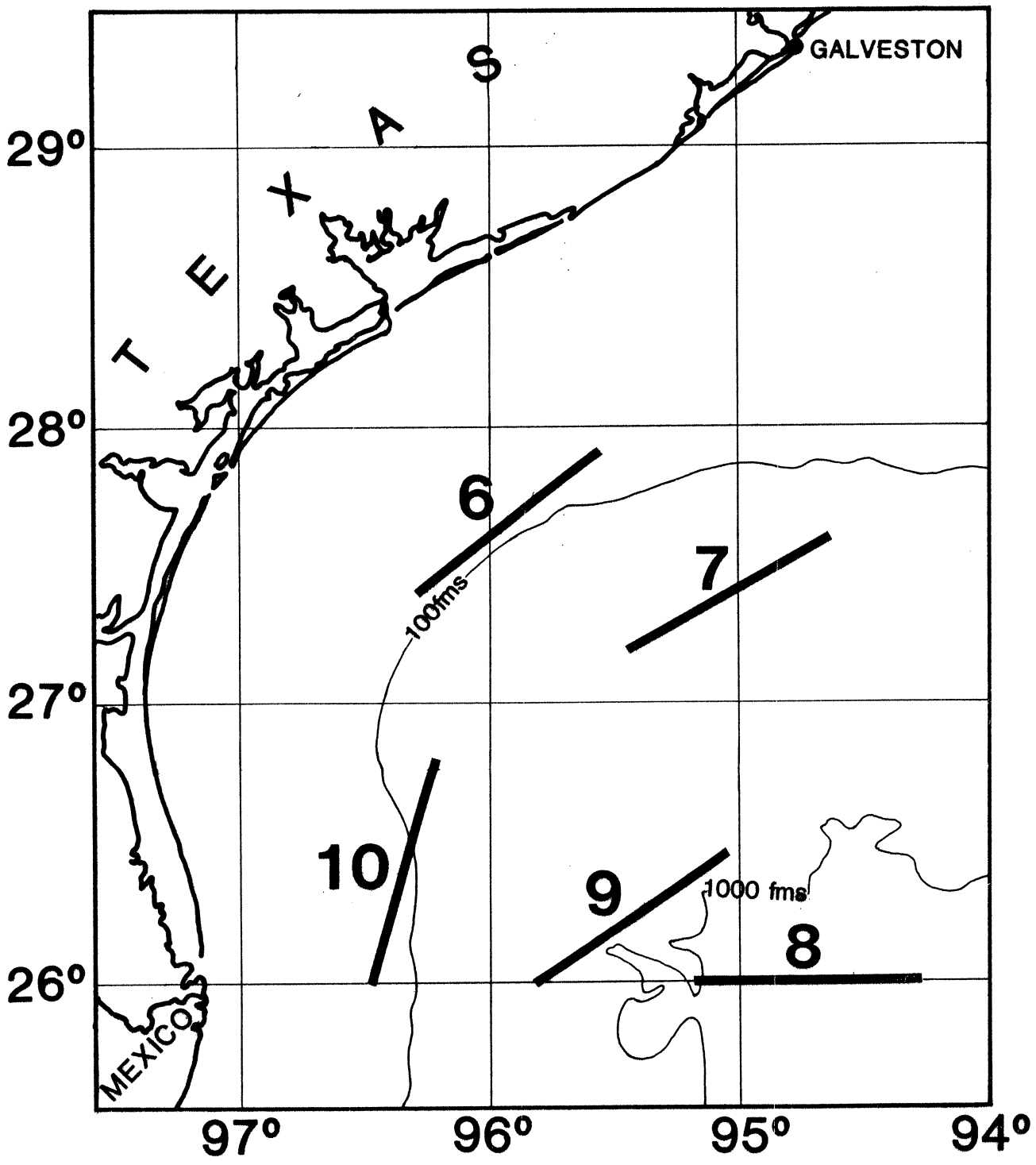

Fig. 1. Location map of the five seismic lines shot during the experiment.

FIELD EXPERIMENT

Seismic Lines

The five seismic lines, Fig. 1, were selected by the sponsor. Each line was approximately 90 km long and its basic setup included four vertical-component OBS's as receivers and 1743 air-gun shots as signal sources. On some of the lines, an OBS with a newly built three-component geophone set was also deployed for testing. Additionally, a few sonobuoys were deployed on each line for supplementary information. Coordinates of the line end points and locations of the successful OBS's are listed in Tables 1 and 2, respectively.

The geometry of the seismic lines, Fig. 2, is different from that of normal seismic reflection lines because of the fixed receiver locations. As an OBS is not tied to the shooting ship, a wide range of offsets, from practically zero to nearly the entire length of a long seismic line, can be achieved. This allows detection of near-vertical reflections as well as wide-angle reflections and refractions from deep layers. In our basic setup, we deployed one OBS near each end and one at about 20 km from each end. This assured a maximum offset of at least 70 km for all OBS's. The sonobuoys filled in the wide gap between the two inner OBS's.

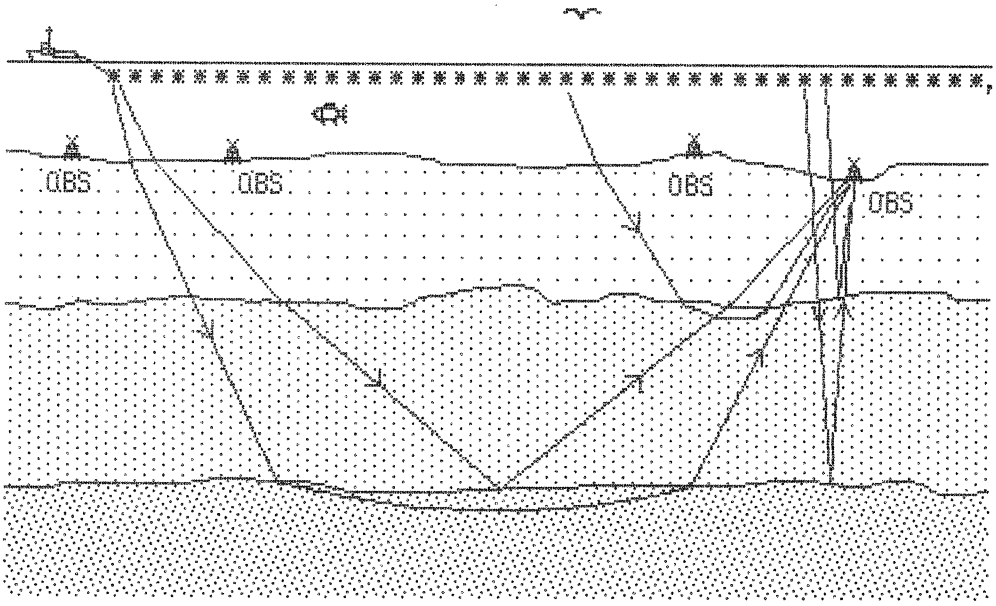

Fig. 2. Geometry of seismic line with four OBS's

Instrumentation

The ocean-bottom seismograph used for this experiment is a very sophisticated seismograph package developed at the University of Texas for detection of seismic signals at the ocean floor. It is an integrated package consisting of the following components: a) a sensor system; b) a set of three preamplifiers; c) a set of three

Table 1. End coordinates of seismic lines

Line	Western (Southern) End		Eastern (Northern) End	
6	27°22.52' N	96°18.31' W	27°55.02' N	95°31.82' W
7	27°10.74' N	95°27.87' W	27°35.82' N	94°38.02' W
8	26°00.15' N	95°12.97' W	26°00.80' N	94°16.19' W
9	25°59.91' N	93°49.38' W	26°27.45' N	95°03.91' W
10	25°59.89' N	96°28.98' W	26°46.35' N	96°13.42' W

Table 2. OBS locations

Line	OBS	Latitude	Longitude	Depth, m
6	1	27°52.75' N	95°35.34' W	67
	2	27°46.15' N	95°45.22' W	74
	4	27°24.19' N	96°16.28' W	140
7	3	27°29.03' N	94°51.41' W	876
	4	27°34.53' N	94°40.74' W	779
	5	27°11.14' N	95°27.25' W	1236
	6	27°11.11' N	95°27.22' W	1236
	7	27°17.00' N	95°15.20' W	1182
	8*	27°17.14' N	95°15.28' W	1182
8	1	26°00.21' N	95°09.78' W	1691
	2	26°00.20' N	94°57.57' W	2727
	3	26°00.87' N	94°30.53' W	3030
	4	26°00.49' N	94°18.33' W	3013
	5*	26°00.88' N	94°30.49' W	3030
9	1	26°00.60' N	95°47.82' W	929
	2	26°06.90' N	95°37.71' W	1253
	4	26°26.73' N	95°05.31' W	1717
	5*	26°20.61' N	95°15.42' W	1385
10	1	26°45.30' N	96°13.74' W	456
	2	26°34.75' N	96°17.28' W	478
	3	26°11.56' N	96°25.19' W	74
	4	26°01.15' N	96°28.71' W	67

*Three-component units

binary-gain-ranging amplifiers; d) a 3-channel signal multiplexer; e) a 12-bit analog-to-digital converter; f) up to 96K bytes of temporary data storage memory; g) a digital cartridge tape recorder; h) a clock; i) an acoustic transponder; j) a release mechanism; and k) a set of recovery aids.

The sensor system is normally made up of one to three geophones, but may include a hydrophone. The binary gain ranging permits a wide dynamic range of over 96 dB. The temporary data storage memory, which is enough to store 48,000 12-bit data words, each with sign, exponent and component identification, is required because the tape recorder must be turned off during data acquisition to avoid vibration noise.

The data acquisition is controlled by three microprocessors for overall system control, clock control and tape recorder control. They are individually programmed to give wide flexibility in data acquisition mode (such as number of channels, sampling interval, record length and timing of recording), compensation of clock drift, formatting of data for recording, and release of the instrument package from the ocean floor.

The electronics subsystems, geophones, the acoustic transponder and strobe lights for recovery aid are contained in a glass sphere, 17 inches (43 cm) in diameter, which is protected by a molded plastic cap. This buoyant package with two radio beacons and bright orange flags constitute the recovery capsule, which returns from the ocean floor after data collection.

On deployment, the recovery capsule is attached firmly to a 4' x 4' (1.2 m x 1.2 m) steel anchor frame by three stiff elastic straps linked by a stainless steel wire, Fig. 3. The bottom of the frame has many spikes, which penetrate the ocean floor sediments to improve seismic coupling. The package is released from the ocean floor for surface recovery by electrolytic dissolution of the stainless steel wire in sea water, triggered by one of three independent means: programmed release controlled by the main clock, preset release initiated by a backup clock and acoustic recall by surface-ship.

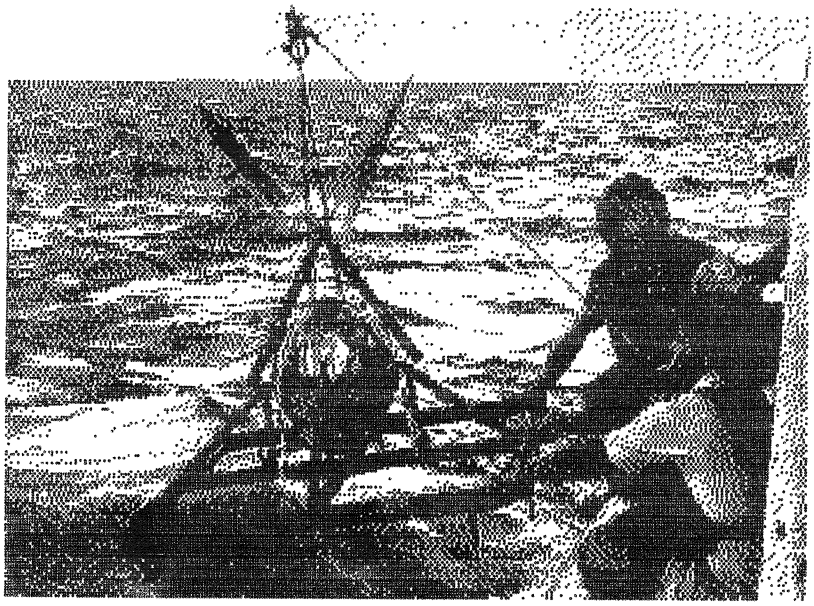

Fig. 3. The Texas OBS being deployed from R/V *Fred H. Moore*.

Field Parameters

Various parameters of the field experiment are listed below:

Source:	Two air guns, Bolt model 800C, 2000 in^3 each, at 2000 psi
Towing depth:	35 feet (11 m)
Repetition rate:	40 s for first pass; 30 s for second pass
Ship speed:	4.9 knots
Shot spacing:	100 m for first pass, 75 m for second pass, producing average spacing of 100 m for single-pass sections (near offset) and 43 m for double-pass sections (far offset)
Receivers:	OBS, 4.5 Hz vertical geophone, Mark Product model L1BU [Test OBS: 4.5 Hz 3-component geophone, Litton model LRS-1011, self-leveling] Streamer, 600 m, 5 channels Sonobuoys
Pass band:	4.5 - 20 Hz
Overall sensitivity:	7.0×10^{-7} (m/s)/DU [2.6×10^{-6} for 3-component]
Recording window:	20.4 s, sliding [13.7 s for 3-component]
Sampling interval:	10.008 ms

Navigation

We used Loran-C as the primary means of navigation to locate each OBS and shot point, supplemented by satellite navigation for absolute refereance. The procedure was to use geographic coordinates as determined by satellite navigation to estimate the additional secondary correction factor (ASF) needed for computation of latitude and longitude from the observed Loran-C TD values for each line. The ASF values thus determined and used for the computation are listed in Table 3.

Table 3. Loran-C additional secondary correction factors

Line	WASF,μs	XASF,μs
6	1.19±0.02	1.2±0.2
7	0.87±0.04	0.6±0.2
8	0.31±0.03	0.9±0.2
9	0.45±0.07	1.1±0.5
10	0.54±0.03	0.5±0.1

When individual TD readings are used independently for each shot, however, their precision is not sufficiently high to allow computation of the relative locations of shot points at high accuracy. Thereore, we first smoothed the entire set of measured TD values using piecewise continuous cubic Hermite functions, and then computed more accurate estimates of TD values at each shot from the smoothed TD functions. Finally, we computed shot coordinates using these accurate TD estimates. We estimate the relative distance between shots to be accurate to better than 1%. However, absolute locations may be off by as much as a nautical mile.

Field Experiment

The experiment was conducted from the R/V *Fred H. Moore*, cruise No. FM-24, from March 20 to April 2, 1984. The ship made four passes over each of the five lines to collect the data. On the first pass, four vertical-component OBS's were deployed sequentially at predetermined locations. On some of the lines (8, 9 and 7-reshoot), an additional OBS with a three-component geophone set was deployed for testing purposes alongside a vertical-component OBS at one of the inner locations. The line was then retraced at 4.9 knots while shooting the air guns at a 40 second repetition rate for the first 901 shots, giving a 100 m shot spacing for the entire 90 km length of the line. All four vertical-component OBS's were programmed to record all of these shots, while the 3-component OBS recorded only a portion of these shots. We also towed a short streamer to collect supplementary shallow reflection data during this pass. After a turn around of the ship, we shot an additional 842 shots in two sections at a 30 second repetition rate, or 75 m shot spacing, during this third pass. The first section shots (902 through 1322) over the first 31.5 km of the line were recorded by the two distant OBS's (OBS's 3 and 4). After a brief transit, the second section shots (1323 through 1743) over the last 31.5 km of the line were recorded by the other two, now distant, OBS's (OBS's 1 and 2). Finally, the line was retraced for the fourth time to recover the OBS's.

In all, five lines were shot. However, one of the lines, Line 7, had to be reshot because only two of the four OBS's on the line worked properly for the first shooting. The reshoot with four additional OBS's (including a three-component unit) at the two missed locations was successful. All four OBS's on Line 10 and all five OBS's on line 8 (including a three-component unit) worked successfully, while one of the four OBS's on Line 6 and one on Line 9 (the vertical-component unit deployed alongside a three-component unit) did not function properly and no data were obtained from these OBS's. Thus, after deployment of 26 OBS's at 20 locations, we collected data from a total of 22 OBS's at 19 locations on five lines during this experiment (Table 2).

DATA PROCESSING

Standard processing of the acquired data consisted of the following steps:

a) Reformatting of the seismic data on cartridge tapes to SEG-Y format: The original OBS data are written on each cartridge tape in a special format to conserve tape usage. The data are reformatted to standard SEG-Y format and are rewritten onto a standard computer tape.

b) Post-cruise recomputation of shot locations: Shot locations are recomputed from the measured Loran-C TD values using the ASF values estimated from comparison with the satellite navigation coordinates as described above.

c) Location (and orientation in case of 3-component unit) of OBS based on water-wave arrival times (and amplitudes): The actual location of each OBS is slightly different from its deployment and recovery locations because of the drift due to existing current and wind. The observed water-wave arrival times are used to determine the actual location of each OBS as well as the exact clock correction at the time of the passage of the shooting ship over the instrument using a least-squares inversion of the arrival times. In the case of the three-component unit, the relative amplitudes together with the arrival times are used to determine simultaneously the location of the OBS, the orientation of the horizontal-component geophones and the clock correction.

d) Merging of navigation data into SEG-Y format tapes: Revised navigation data based on the recomputed shot and OBS locations and clock drift are merged into the initial SEG-Y format tapes described above.

e) Coordinate rotation (3-component unit): The horizontal components of three-component data are rotated into radial and tangential components using the instrumental orientation as determined in step c) above.

f) Stacking of traces into uniform offset bins: The acquired seismic traces are not evenly spaced in offset because the speed of the ship varies from time to time while the shooting must be done according to preset time schedule and not by distance. To facilitate interpretation of record sections, we 'stacked' the traces into 100 m bins using a stacking velocity of 6 km/s. The offset range for this stacking was short enough (about ±60 m) so that attenuation of arrivals of phase velocities different from 6 km/s was negligible. For sections of lines where data from two passes are available and in cases where two OBS's are deployed at the same location, the multiple data are also stacked together to improve the signal-to-noise ratio.

g) Plotting of record sections: The binned traces were plotted to produce the basic seismic record section plots.

h) Deconvolution: Since the air guns used for this experiment are not tuned, several cycles of bubble pulses appear following each arrival. Though these regular cyclic arrivals are quite advantageous for recognition of weak refraction arrivals at far distances, they interfere with identification of reflections at near ranges. In order to reduce the bubble pulses, we apply deconvolution to the near-offset (up to 20 km) data to be used for reflection moveout analysis.

Deconvolution filters based on either the bubbled water wave arrivals or the entire trace may be used with satisfactory results.

The processed products d) through h) were then used for further processing and interpretations. Figures 4a through 4e (on fold-out pages) show reduced copies of seismic record sections. The multichannel data on each line are also stacked into 100 m bins and are displayed in a filtered and deconvolved single-fold section.

The following figures are on the fold-out pages:

Fig. 4a. Line 6 seismic record sections.

Fig. 4b. Line 7 seismic record sections.

Fig. 4c. Line 8 seismic record sections.

Fig. 4d. Line 9 seismic record sections.

Fig. 4e. Line 10 seismic record sections.

LINE 6

SOUTHWEST

NORTHEAST

DISTANCE, KM

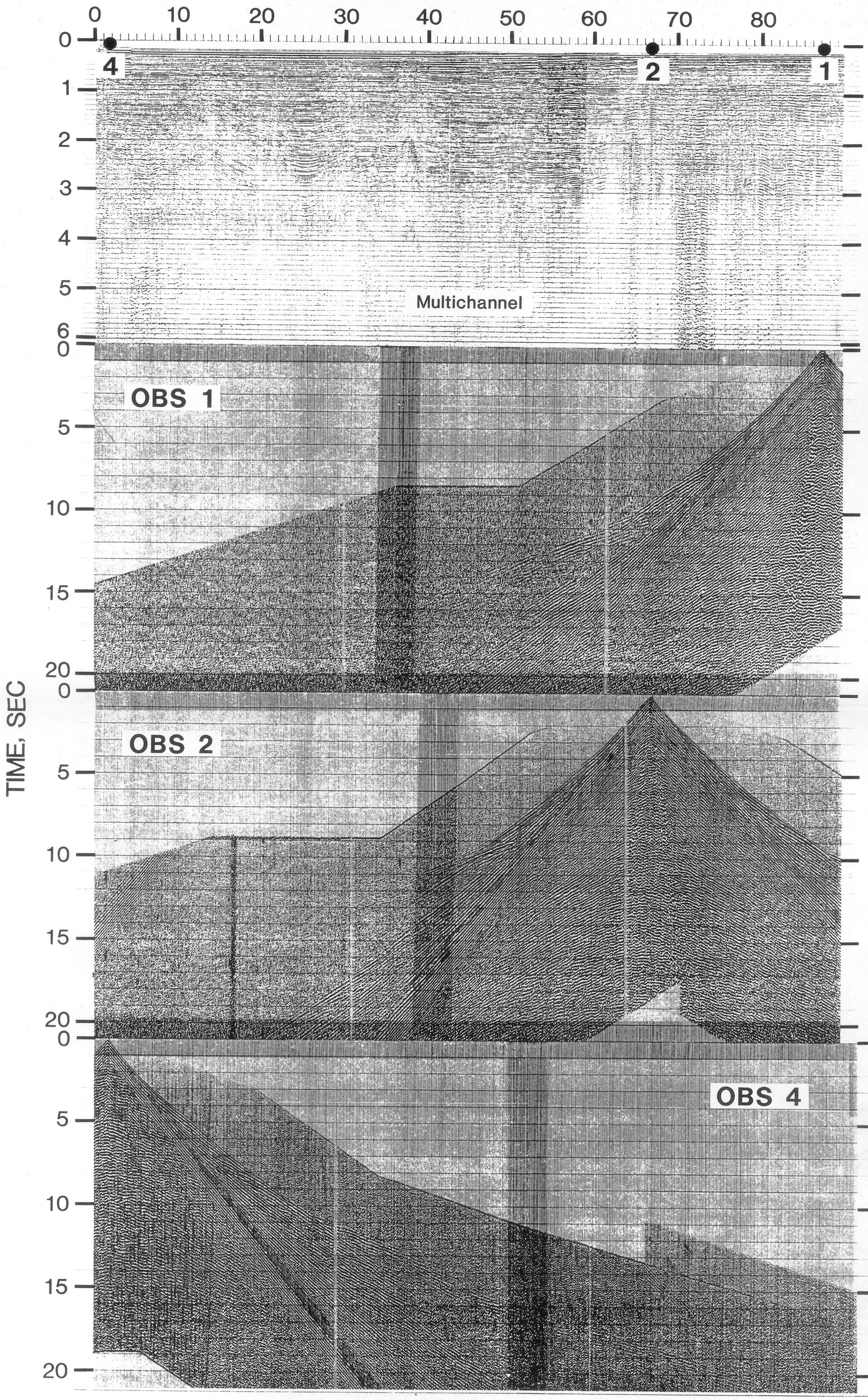

LINE 7

SOUTHWEST

DISTANCE, KM

NORTHEAST

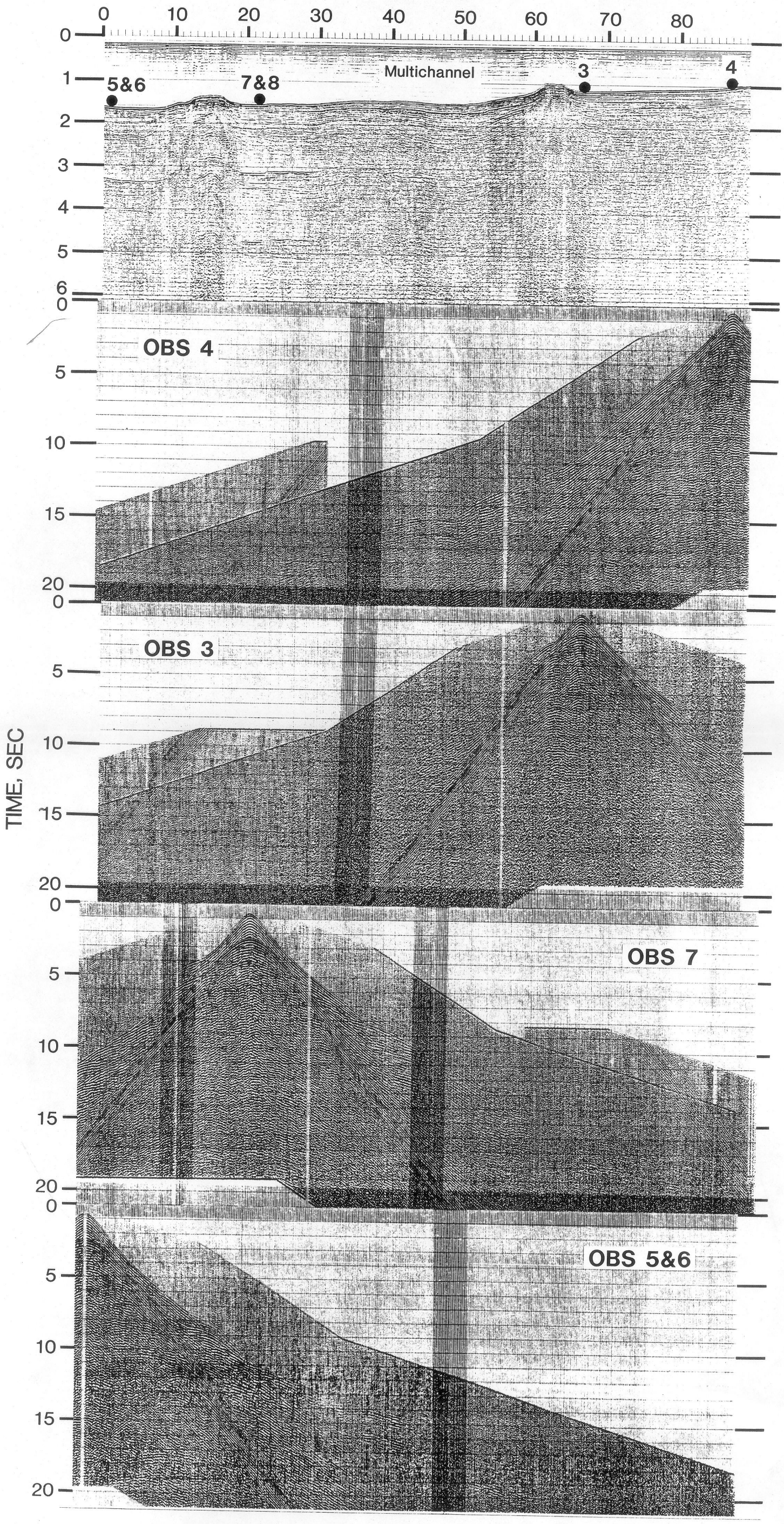

Line 8

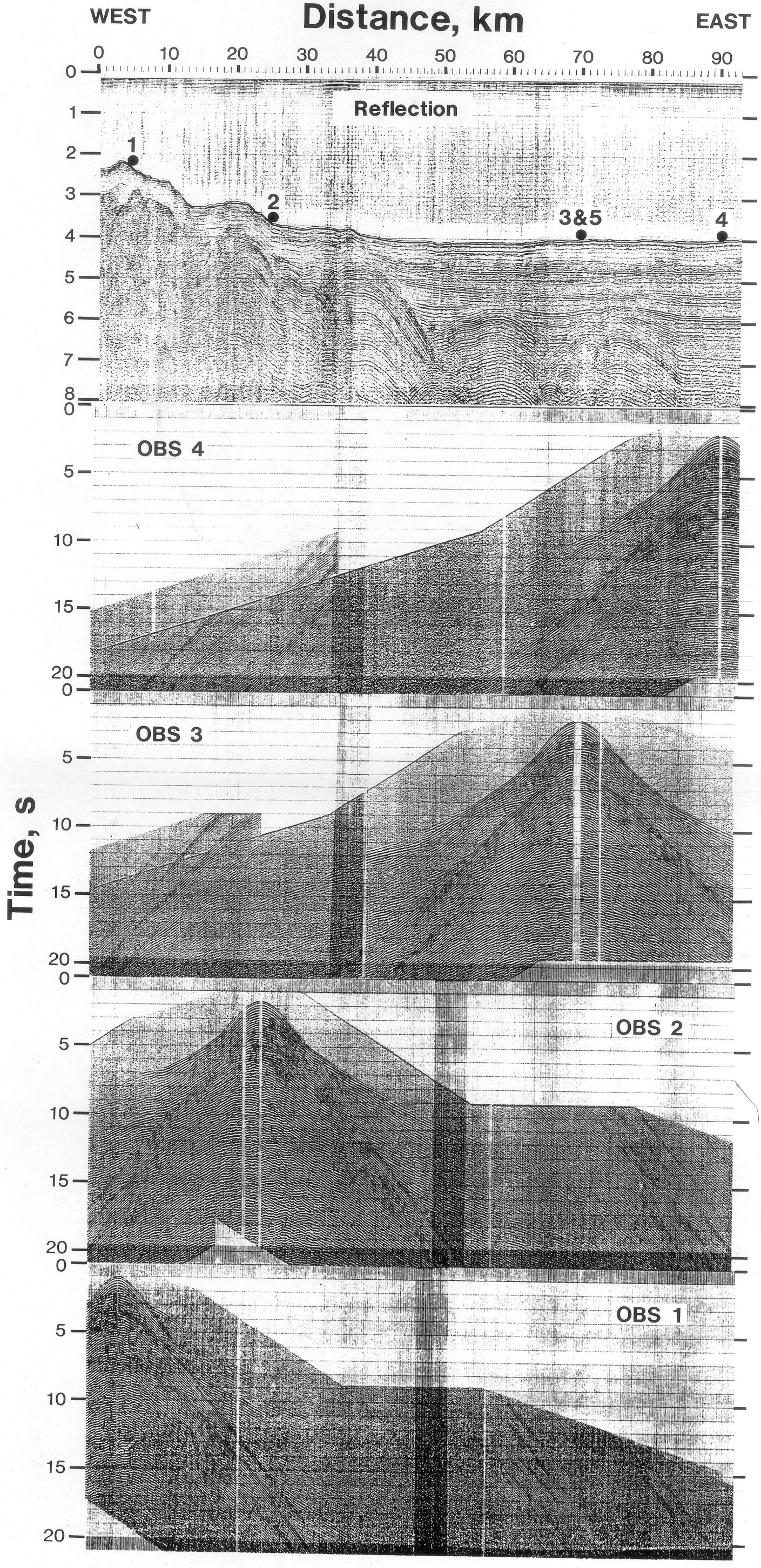
WEST
Distance, km
EAST
0
10
20
30
40
50
60
70
80
90
Reflection
1
2
3&5
4
OBS 4
OBS 3
OBS 2
OBS 1
Time, s
0
1
2
3
4
5
6
7
8
0
5
10
15
20

LINE 9

SOUTHWEST

DISTANCE, KM

NORTHEAST

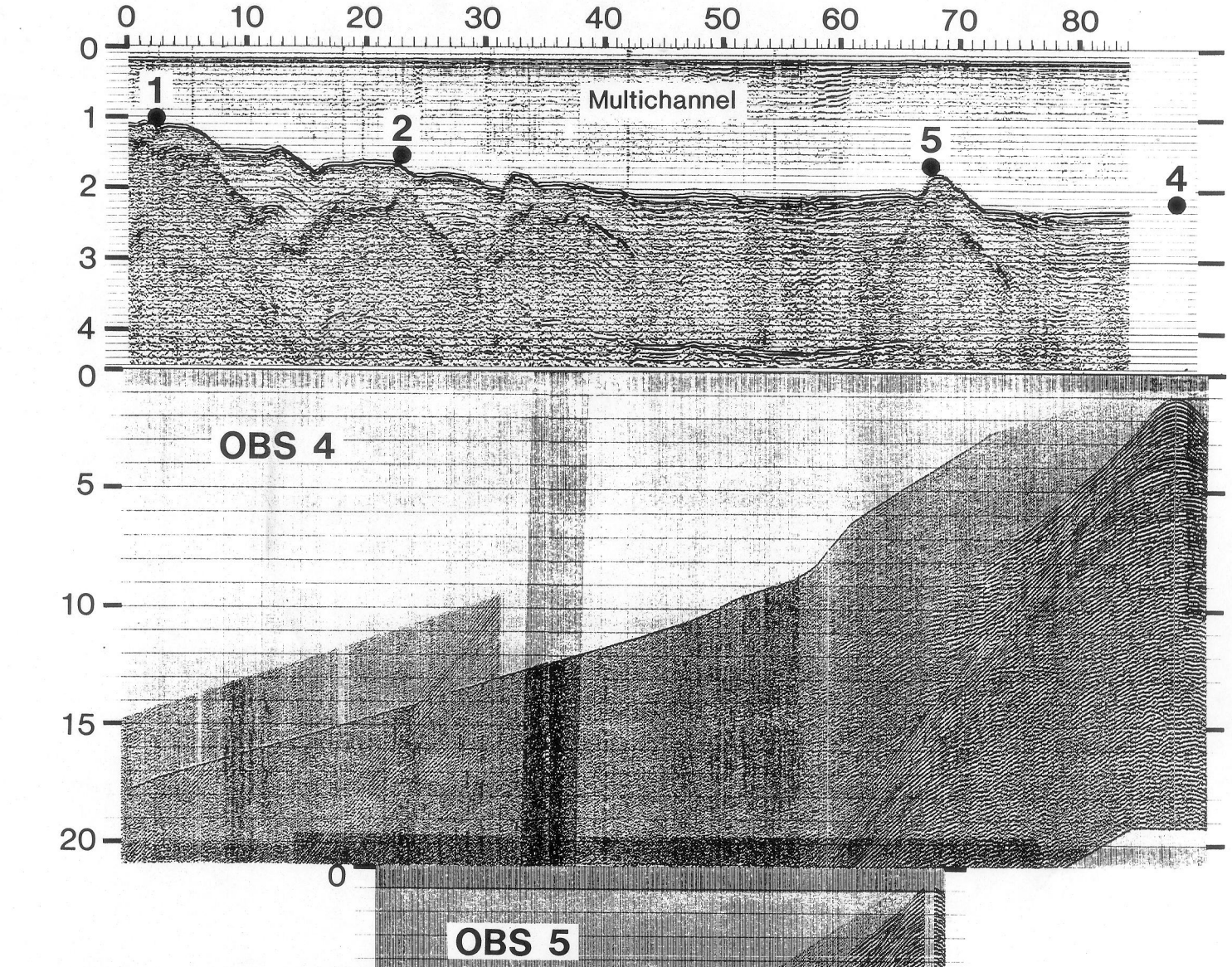

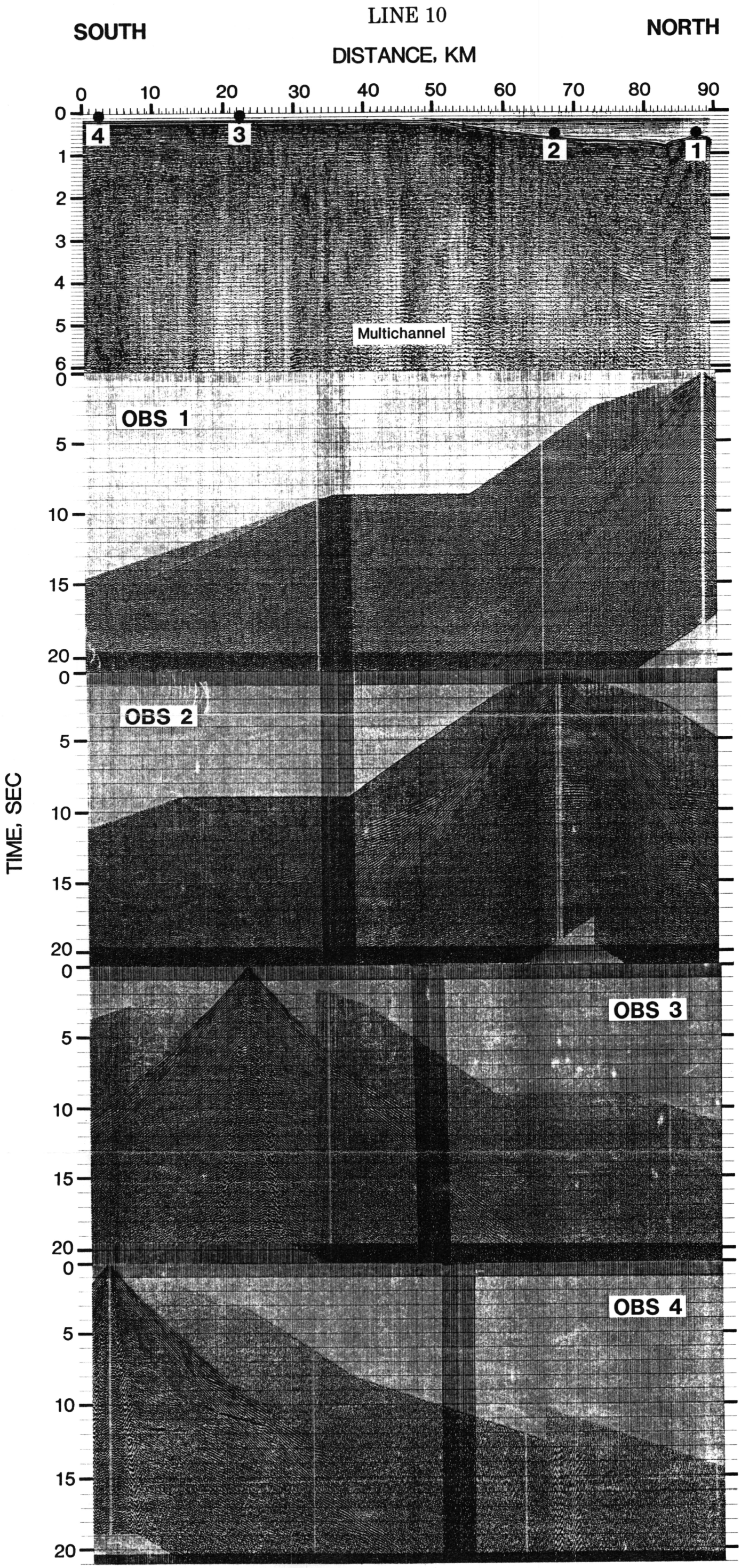
LINE 10
SOUTH
NORTH
DISTANCE, KM
0
10
20
30
40
50
60
70
80
90
4
3
2
1
Multichannel
OBS 1
OBS 2
OBS 3
OBS 4
TIME, SEC
0
1
2
3
4
5
6
5
10
15
20

ANALYSIS AND INTERPRETATION

Analysis Methods

There are several conventional and unconventional methods to use in analyzing and interpreting the kind of seismic data acquired in this experiment. The simplest and most common method for large offset refraction data is the interpretation in terms of flat, constant-velocity layers as calculated from the slope and intercept time of refracted arrivals, especially of those which are observed as first arrivals. If the structure is not too complicated, this method will give a rough estimate of the velocity-depth profile. The method, however, breaks down if there are velocity inversions or if large lateral velocity variations exist.

Near-vertical reflection data can be analyzed using moveout of arrivals with offset as in ordinary reflection work. The larger offsets available in this experiment compared with normal reflection surveys allow us to determine interval velocities more accurately, although the large offsets require us to account for non-hyperbolic moveout.

Since the data acquired in this experiment are of sufficiently high spatial density and since they cover a wide offset range including both pre-critical and post-critical reflections, they can be slant stacked successfully into the tau-p (intercept time vs. ray parameter) domain. The transformed data can be inverted to obtain bounds on the velocity-depth function.

These procedures, however, assume that either the structure is horizontally homogeneous or the lateral variation is at most gradual. Unfortunately, neither assumption is valid for most areas covered in the present experiment since parts of all five lines of the experiment lie over structures that exhibit a high degree of lateral heterogeneity. The results obtained by assuming one dimensionality only gives very approximate solutions.

Based on our experience with this type of data for the last two years, the analysis method we have found most successful is a combination of various one-dimensional techniques with two-dimensional (2-D) ray tracing. Also essential in this analysis is an access to multichannel reflection data, which we now take regularly with all our air-gun/OBS experiments.

The procedure we followed can be summarized as follows:

a) First, we pursue one-dimensional analysis as far as the data allow. This includes conventional layered-model interpretation of refraction arrivals, applicable for both shallow and deep structures; direct inversion of first arrival times into a continuous velocity profile for shallow structures; moveout analysis of pre-critical reflection data for interval velocities, generally useful down to about 10 km depth; and if data are favorable, inversion of tau-p slant stacked data for velocity bounds.

b) On a multichannel reflection record section, identify major reflecting interfaces and measure two-way vertical travel times to these interfaces at key locations. Then, using the velocities as determined in step a) above, convert the time section into a velocity section. This will give the initial two-dimensional model for the shallow structure near each OBS.

c) Examine the OBS record section and identify any unusual arrivals, such as reflections from the top of a salt intrusion and refractions through the salt. The initial model from step b) above need be modified to accommodate these unusual arrivals.

d) Using the result of step c) above as a starting model, shoot a set of rays in reverse direction, originating at each OBS location and ending at shot points near the sea surface, and compute distance and travel time for each ray. Compare the computed travel times with observed travel times, adjust the model accordingly and repeat the procedure until a satisfactory fit is obtained for all identifiable arrivals. We also pay attention to any focusing and defocusing of rays, which should be manifested in the observed amplitudes. This step should give a satisfactory shallow structural model near each OBS location.

e) Once a satisfactory near-OBS shallow structure is constructed for each OBS location, add deeper layers based on the information gained in the first step to make a model for the entire line. Then shoot another set of rays that penetrate through the shallow structure and appear at large offsets. Compare them with observations and adjust the values to arrive at an acceptable model of the deeper structures.

The following line-by-line interpretations reflect the difference in approach and style of individual interpreters. However, we have tried to preserve consistency among lines.

Line 6 Interpretation (*cf.* Figs. 4a and 5)

Line 6 is a strike line located in the northwestern corner of the study area in shallow water on the continental shelf. Since the regional subsurface structure usually changes relatively little along strike, interpretation of strike lines is generally more straightforward than dip lines, and this line is no exception. The records of OBS's 1 and 2 appear quite similar to each other, while that of OBS 4 appears slightly different from the others.

In interpreting the shallow subsurface zone, it was sufficient to assume a velocity gradient rather than discrete layering. At intermediate depths, I identified three reflectors. It is interesting to note that these reflections are barely visible at near offsets because of strong shallow water reverberations. None of these reflectors can be identified on the multichannel records. The reflections become prominent at wide angles, where they merge with the refracted arrivals. Starting from far offsets they can be traced back to zero offset, clearly showing an advantage of far-offset data acquisition.

Matching of the shapes of the observed time-distance curves of these reflections with theoretical curves provides excellent control over the depths of interfaces and the velocities of the layers in the intermediate depth range. At OBS's 1 and 2, only the deeper two of the three reflectors can be identified with certainty. From the observed velocities, we interpret the upper of these two reflectors, located at 7 to 8 km depth, to represent the middle Cretaceous unconformity (MCU) and the lower of the two, located at 12 to 15 km depth, to represent the basement.

One further prominent feature common to all three OBS records on this line is a refracted arrival of apparent velocity of 7.2 km/s . This arrival is offset by about 2

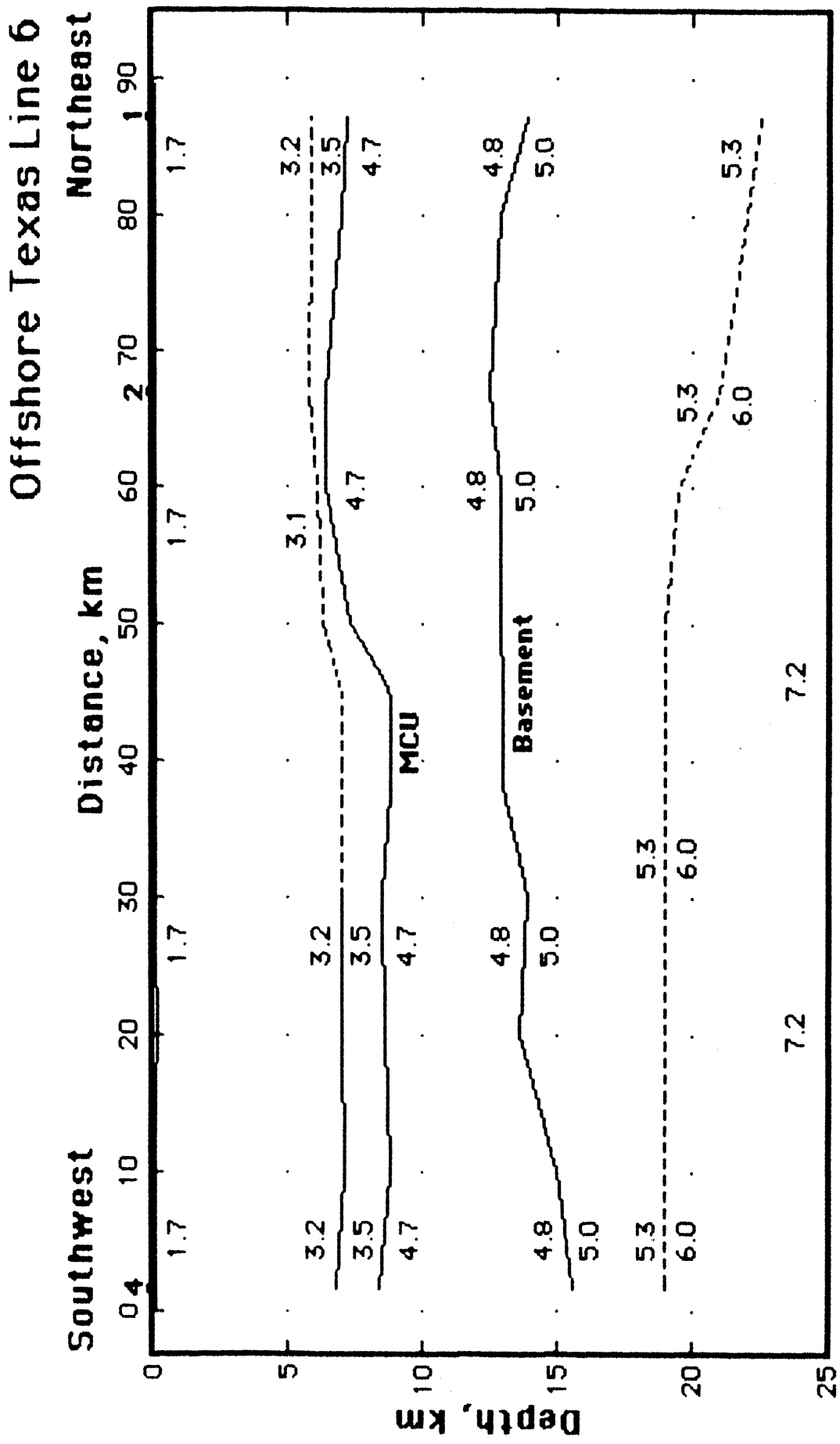

Fig. 5. Line 6 structural profile.

seconds from the deepest of the three wide-angle reflections, interpreted as the basement reflection above. I modeled this large delay by introducing a layer of relatively low velocity gradient below the deepest reflector (basement). Note that we did not observe any reflections from the bottom of, or refractions from within, this upper crustal layer. Instead, its thickness and velocity are solely inferred from the observed delay time of the 7.2 km/s lower crustal arrival. Hence, the deeper structure is not as well constrained as the features at intermediate depths. Since the 7.2 km/s arrivals at OBS's 1 and 2 are observed later than that at OBS 4, I conclude this lower crustal layer to be dipping towards the northeast. The depth to the top of this layer ranges from 19 km at the southwestern end of the line to 23 km at the northeastern end of the line
(J.O.)

Line 7 Interpretation (*cf.* Figs. 4b and 6)

Line 7 was run on the upper continental slope of the northwestern corner of the Gulf of Mexico in .75-1.25 km (2500'-4100') water depths. It was oriented NE-SW, parallel to the Texas coast, approximately 100 nmi south of Galveston, Texas. The line consists of 4 OBS records and associated 4-fold multichannel streamer data.

The multichannel section is displayed in Fig. 4b by filtered, deconvolved near-trace data only. They indicate the following elements: a water bottom ranging from 1.0-1.6 s 2-way travel time; several strong water bottom multiple packages; two narrow structures at shallow depths within the sedimentary section; at least a minor degree of structure along the center portion of the line (roughly 30-50 km, Fig. 4b); and, except at the shallow structures, 1.5-2.0 seconds of discontinuous, subparallel reflections of relatively uniform amplitude and frequency.

The sections from the 4 OBS's generally exhibit the same type of shallow record; i.e., except for the disruptive effects of the shallow structures, the first few seconds of data contain strong multiples, no well-defined reflection arrivals, and only a few poorly defined reflection arrivals. With the exceptions of OBS's 3-SW and 7/8-SW, however, the refractive envelopes (first arrivals) for each shallow section are well resolved. If the sloping water bottom is taken into account, a one-dimensional layer analysis can be made using the phase velocities and intercept times of these refracted arrivals. Because of the shallow structures, the lateral velocity contrasts associated with them, and the deep central structure, reflection-velocity analysis and 2-D ray tracing were primarily used to analyze this line.

The first well-defined reflection surface, correlative across all four OBS sections, is interpreted as a middle Cretaceous unconformity (MCU), a prominent, basin-wide seismic horizon. We can roughly categorize these reflection arrivals as "vertical", within ±5 km offset distance; near-vertical, at about 5-15 km offset; and wide-angle, at about 15-25 km offset on either side of an OBS. Because of ringing and water-bottom and internal multiples, no unambiguous vertical reflections are identified. There are, however, near-vertical and wide-angle MCU arrivals on the OBS 3 and 4 records and wide-angle MCU arrivals on OBS's 5/6 and 7/8; refractions from the underlying layer are observed on OBS's 4, 5/6 and 7/8. The shallow-section refractions and few available reflections, plus the MCU reflections constrain the interpreted Line 7 structure down to and including the MCU. The deep central structure is modeled here as topographic relief on the MCU, possibly due to mobilized, non-diapiric evaporites. This relief is indicated in the OBS records mainly by the early arrival times of the refractions emerging from the underlying interval. Refractions from the slow, overlying unit are

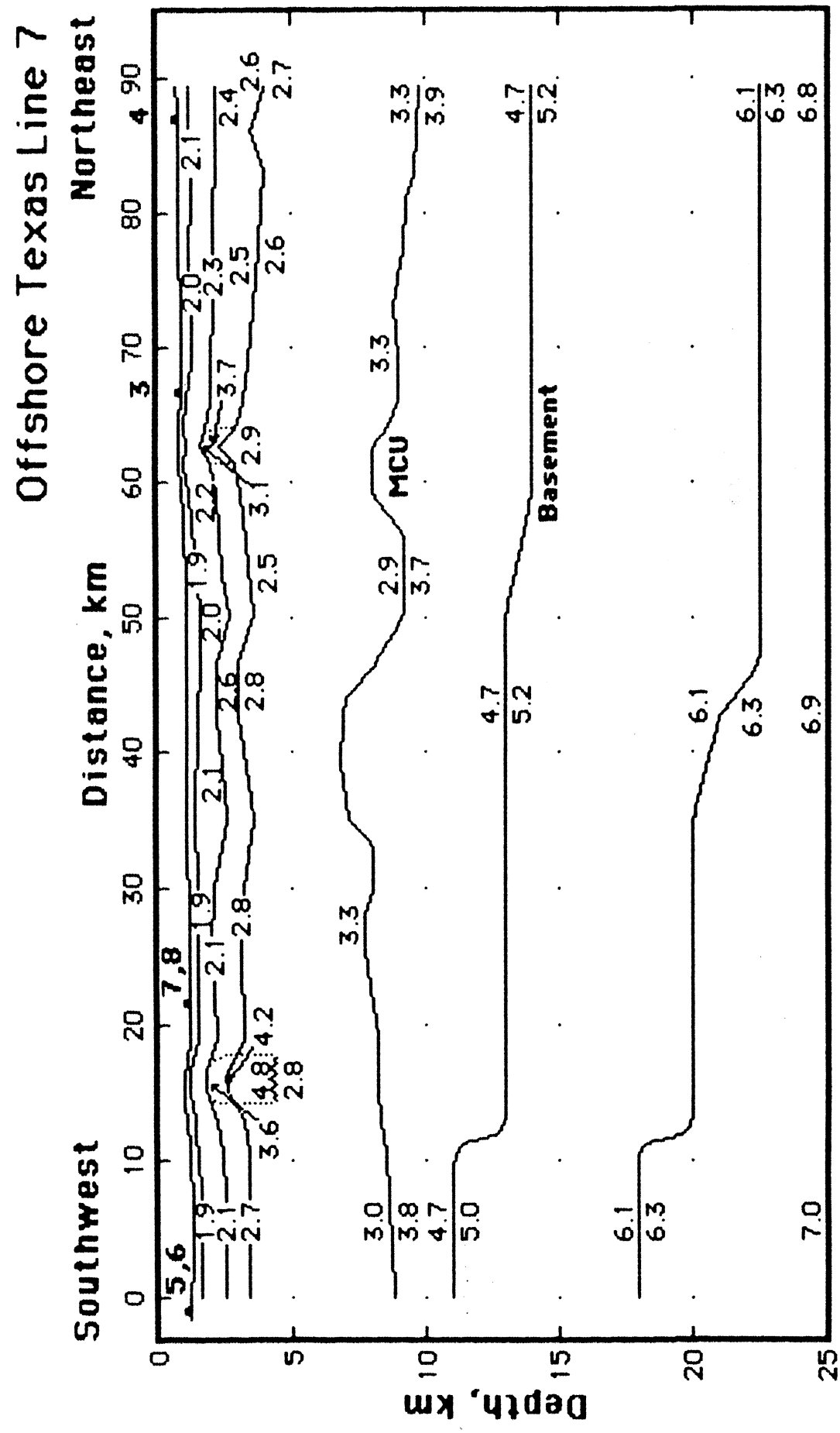

Fig. 6. Line 7 structural profile.

also affected by the reversal of dip on this structure. In the record for OBS 5/6, for instance, the farthest refracted arrivals from this unit overlie the refractions from below the MCU. The velocity of the unit underlying the MCU is estimated by means of the arrival times and phase velocities of refractions from the underlying interval and by the wide-angle reflections from the top of basement.

The top of basement itself is considered to be the first surface interpretable beneath the MCU. As noted above, the surface is resolved by means of wide-angle arrivals cross-cutting or truncating the MCU wide-angle reflections and by the arrival times of refractions from the underlying interval.

The velocity of the underlying interval, the depth of the intra-basement surface (18-23 km), and the velocity of the deepest modeled interval are constrained by a combination of factors: refraction phase velocities, arrival times, a wide-angle reflection on OBS 7/8-SW, and the need to cut off refraction arrivals from the interval immediately underlying the basement surface.

Overall, the sedimentary section, 10-13 km thick on this line, does not generate a well-stratified record, with clear sets of seismic horizons, in either the multichannel or OBS records. This indicates that the column here is most likely not composed of differentiated sand and shale strata. Rather, it consists of relatively homogeneous sediments and, judging by the relatively low interval velocities, contains a significant percentage of deep-marine shales.

The two shallow, narrow piercement structures are modeled with velocities appropriate for dirty salt. They are shown here as not being continuous to depth. This may be the actual case, or they may be too thin at depth to be resolved by our data. In either case, movement continuing into Pleistocene time was likely.

The basement surface dips to the northeast, and an intrabasement surface is interpreted here. Judging by the basement velocities, depths, and minimum thickness, we expect that this is a section of transitional, originally continental crust. Since no mantle velocities were observed in these data, none are suggested here. Based on the velocities that we used here for the section between 20 and 25 km, a lower crustal boundary is probably no shallower than 30 km.
(F.J.S.)

Line 8 Interpretation (*cf.* Figs. 4c and 7)

Line 8 is an east-west line on the 26° N parallel crossing the foot of the continental slope. The eastern half of this 93 km line is on the continental rise at the northwestern corner of the deep Gulf with a nearly constant bathymetric depth of about 3000 m; while its western half shows an irregular rise to the west to a depth of about 1700 m, crossing three evenly spaced and successively higher ridges.

We proceeded with the analysis of this line first by interpreting the shallow (down to about 10 km depth) structure in its eastern half, where the structure is simpler, and then by extending it to the west, where it becomes more complex. After the shallow structure is well defined, we proceeded to interpret the far-offset arrivals for deeper structural definitions. The following description generally follows this procedure. The cited distances are measured from the western end of the line.

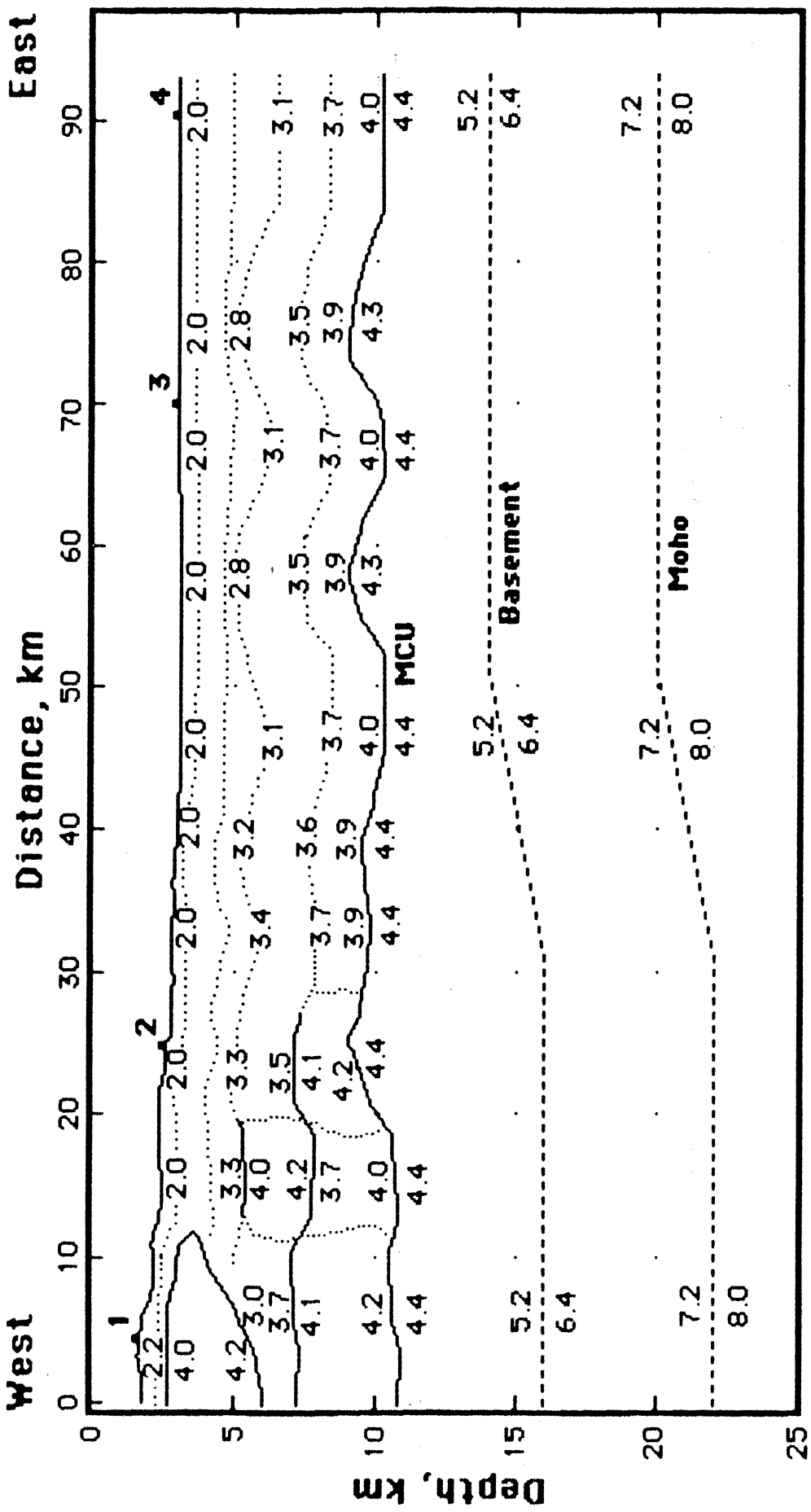

Fig. 7. Line 8 structural profile.

1) 84-93 km: The structure under this easternmost 9 km of the line is nearly completely flat. Any of the one-dimensional analysis techniques works for this region. The moveout analysis of pre-critical reflections observed at OBS 4 fairly well defines the velocity profile in the sedimentary column down to a depth of about 12 km. Prominent seismic reflectors are found in the section at depths of 3.8 km, 4.4 km, 4.9 km, 6.5 km, 10.5 km and 12. 4 km. From the character of the wide-angle reflection, we interpret the reflector at 10.5 km to be the middle Cretaceous unconformity (MCU). The seismic P velocity jumps from 4.0 km/s just above MCU to 4.4 km/s below.

2) 50-84 km: This is the part of the continental rise where the bathymetry is nearly level but structures are present at depth. The top 2 km of the sub-bottom sediments (down to a depth of about 5 km) is undisturbed and is an extension of the upper layers underneath OBS 4. Below 5 km depth, there exist two anticlines separated by about 18 km (assuming that they run perpendicular to the line). Although they appear clearly on the multichannel reflection record section, the vertical velocity variation as determined from OBS data by 2-D ray tracing of refraction (diving wave) arrivals is nearly independent of the structure along the line (see Fig. 7). The depth, rather than the sedimentary facies, appears to determine the velocity variation in this sedimentary section. The MCU reflections are well observed on the OBS records throughout this section of the line. Two-D ray tracing of these arrivals shows the topographic relief of the MCU to be about 1 km beneath each of the anticlines. Whether these two anticlines are caused by salt below the MCU, whose upward movement stopped sometime ago, cannot be determined from the seismic data alone because seismic velocity below the MCU is indistiguishable from that of salt.

3) 30-50 km: This section of the line marks the foot of the continental slope. It is also intermediate in structure between those to the east and west. The anticline, unlike those to the east, perturbs the sea bottom, indicating that it may even be active in Holocene time; while no large zones of salt intrusions, like those to the west, are found in the upper 7 km of the sedimentary section. However, the seismic velocities in the middle sedimentary section between the distances of 30 to 40 km are slightly higher than those to the east, indicating that there may be some changes in lithology, possibly small inclusions of salt in the structure.

4) 0-30 km: This is the most complex section of the line. It is underlain by several large inclusions of salt of dimensions on the order of 7 to 10 km laterally and 2 to 4 km vertically. One of them comes to within 1 km of the sea bottom near the western end of the line. Their seismic P velocities are in the range of 4.0 to 4.2 km/s. Locked among salts are sediments, whose velocities, nevertheless, are again slightly higher than their counterparts under the continental rise to the east, suggesting that even these sediments include small patches of salts in them. The blocky salt model of Fig. 7 may not be the only interpretation, though it satisfies the 2-D ray tracing results. Another possible interpretation may a series of inclined zones of salt of varying thicknesses. This model may be more appealing to geologists in terms of their mobility through the structure. The MCU boundary appears to deepen from east to west in this part of the line, possibly due to withdrawal of salt masses.

5) Basement: Arrivals from a horizon below the MCU are observed at all OBS's except OBS 1 from shots over "windows" of better seismic penetration, generally through the basins. With appropriate assumptions of the mean velocity between the MCU and this horizon and of the velocity below the horizon, the depth to the horizon can be estimated. Using 4.8 km/s and 6.4 km/s, respectively, for these velocities, the depth to the horizon under the eastern half of the line is at about 14 km. It deepens in

the western part of the line to about 16 km. This horizon may be interpreted as marking the top of the crystalline basement.

6) Moho: The deepest arrivals observed on OBS 3, and possibly also on OBS 4, from shots to the west show a phase velocity of 7.1 km/s. A horizontal layer assumption will place the layer at a depth of about 18 km. However, considering the dip of the top of the basement to the west, it is more reasonable to interpret this velocity to be an apparent velocity lower than the true velocity. If we assume the true velocity to be about 8 km/s or slightly above appropriate for the upper mantle, the estimated depth to the layer becomes about 20 km. This interpretation implies that we are observing refractions from the Moho, which dips towards the west.

This interpretation of Line 8 is consistent, at its eastern end, with our earlier results from a line east of this line that was entirely on the continental rise giving a credence to this interpretation. The eastern end of the line is underlain by what appears to be oceanic crust about 6 km thick under 11 km of sediments. The sedimentary section thickens to the west under the continental slope. The variation of the thickness of the crust, however, cannot be determined from the present data. (Y.N.)

Line 9 Interpretation (*cf.* Figs. 4d and 8)

Line 9 is located on the northwest slope of the Gulf of Mexico in water 750-1650 m deep. This line trends NE-SW, oblique to the shore line but paralleling the local bathymetric contours. Overlying the Rio Grande Embayment Tertiary depocenter, this upper continental slope region features abundant ridge-like diapiric salt bodies.

The associated multichannel seismic section shows evidence of considerable lateral heterogeneity in the shallow structure. The southwestern half of the line overlaps a large, irregular structure exhibiting a strong subbottom reflector with extensive relief, overlain by deformed sediments with subdued but elevated sea floor topography. The northeastern half of the line is characterized by flat-lying sediments punctuated by an isolated dome. Steeply dipping reflections merge with reflections off the flank of this feature, characteristic of side echoes off seafloor structures extending out of the vertical plane. This indicates that this apparent dome is most likely a spur of the elongate salt intrusive mapped by Martin[1] just to the northwest of the line. Given the less than optimum water depths, multiples obscure arrivals deeper than 3 to 4 seconds of two-way travel time.

We recovered data from four OBS's on this line including one 3-component instrument. OBS's 1 and 2 were located on the massive structure at the southwest end of the line. The 3-component instrument (OBS 5) was positioned directly on the small dome while OBS 4 was situated on relatively flat-lying sediments. Unfortunately, a major characteristic of the OBS records is the disruptive effect of the salt bodies in terms of defocusing of the acoustic signal. However, with the OBS data we were able to detect sub-salt arrivals which are obscured by water bottom multiples in the standard multichannel section.

---

[1]Martin, R., 1980, Distribution of salt structures in the Gulf of Mexico: Map and descriptive text, USGS Map MF-1213.

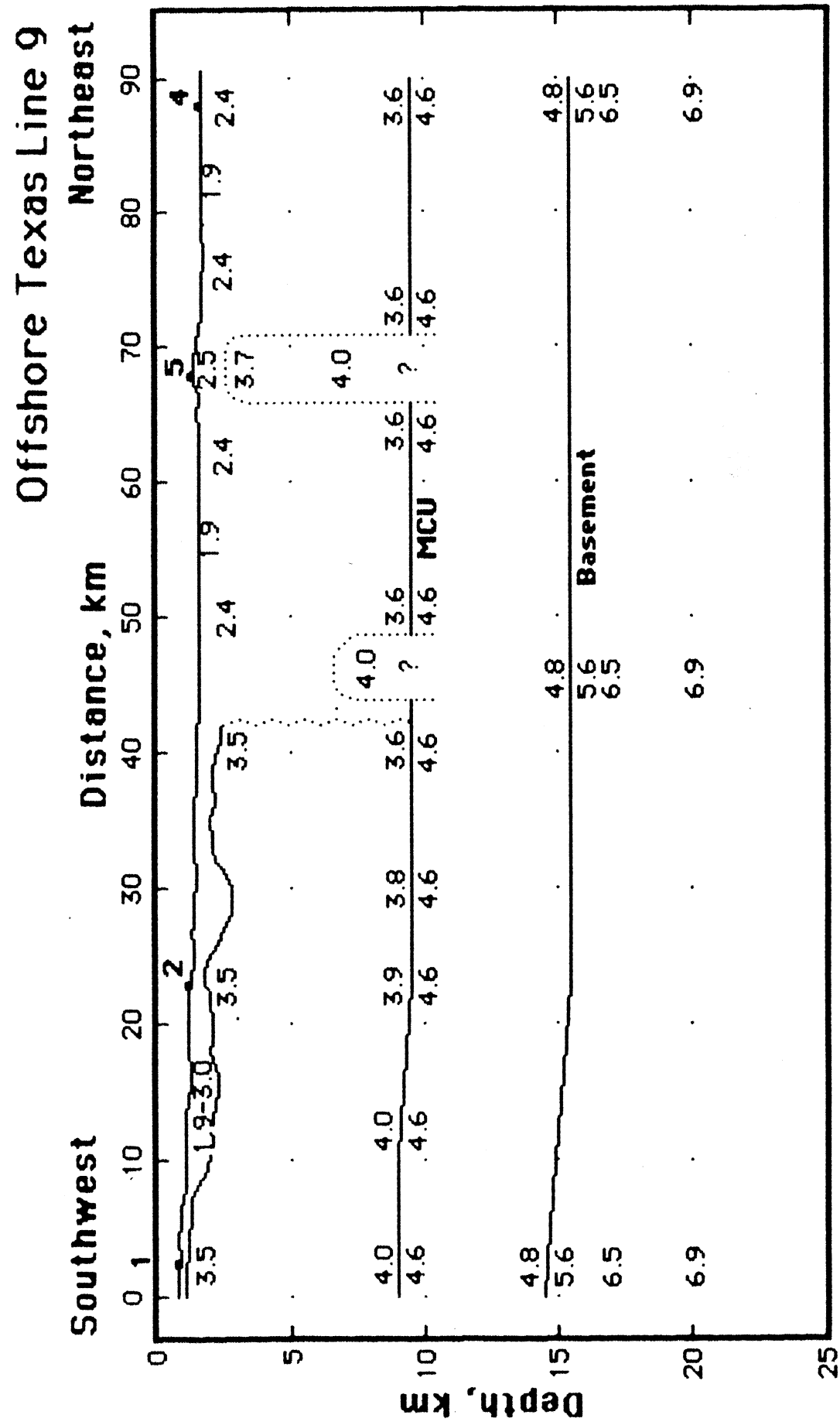

Fig. 8. Line 9 structural profile.

Our analysis began with the shallow sedimentary section exemplified by the flat-lying stratigraphy on the northeastern half of the line. Using one-dimensional modeling on data from OBS 4, we established a smoothly varying velocity structure devoid of prominent, shallow reflections. Observed velocities run from 1.6 km/s at the sea floor to 1.9 km/s at 2.0 km depth to 2.3 km/s at 2.4 km depth. Velocities reach 3.6 km/s at the middle Cretaceous unconformity (MCU) at a depth of 9.5 km. Sedimentary sections overlying the salt bodies exhibit high velocity gradients although velocities are poorly resolved given their small thickness and deformed nature.

At this point, we applied two-dimensional ray tracing to our model. The tops of the salt structures are well defined by strong reflections in the multichannel data and in the data recorded by OBS's 1, 2 and 3. MCU and basement reflections can be traced from their associated wide-angle reflections and refractions back to small offsets at all four OBS's.

Results of our two-dimensional modeling indicate that the one-dimensional model for OBS 4 is representative of the northeastern half of the line. This section consists of a thick, laterally homogeneous pile of sediment overlying the flat MCU at a depth of 9.5 km below sea level. This section is disrupted by a salt column capped by sediments with velocities of 2.5 km/s. The dimensions of the salt column are not well constrained; a vertical reflection from the bottom of salt is not evident although a reflection from MCU can be traced beyond a few kilometers of offset.

The other half of the line is dominated by the massive salt feature. Much of the scatter of arrivals observed at OBS's 1 and 2 is explained by the seafloor and salt topographies which are highly three-dimensional. We modeled this structure with velocities ranging from 3.5 to 4.0 km/s, placing MCU at a depth of 9.0 km. No reflections from the bottom of salt are noted in the OBS data while MCU appears as a distinct event. Although we cannot exclude the presence above MCU of low velocity sediments interspersed with higher velocity salt (as in Line 8), the associated jumps in travel times for refracted energy turning in this region must be small. Therefore, MCU could be up to a few hundred meters shallower. The northeastern end of the massive structure is poorly constrained and may be bounded by small diapirs.

Depths to interpreted basement are controlled by wide-angle reflections near each OBS with refractions fixing the depth between OBS's 2 and 3. Basement dips gently from 14.5 km under OBS 1 to a constant 15.5 km between OBS's 2 and 4. Velocities increase rapidly from 5.6 to 6.5 km/s in the upper few kilometers of basement. Apparent velocities up to 6.9 km/s are observed at OBS's 1 and 2 to an estimated depth of 23 km. No coherent subbasement reflections or mantle arrivals were noted.
(K.M.)

Line 10 Interpretation (*cf.* Figs. 4e and 9)

Line 10 trends NNE-SSW about 40 miles off the southern Texas coast and surveys the northern portion of the Rio Grande Embayment. The southern half of the line is located on the shelf in 70 m of water, while the northern half of the line covers the upper continental slope to about 500 m water depth.

The multichannel data indicate a thick sedimentary prism including a solitary shallow salt diapir at the northern end of the line. Within the shelf section the reflections are usually discontinuous with uniform amplitude and frequency. The structure consists of broad, gentle anticlines. The upper slope is underlain by an

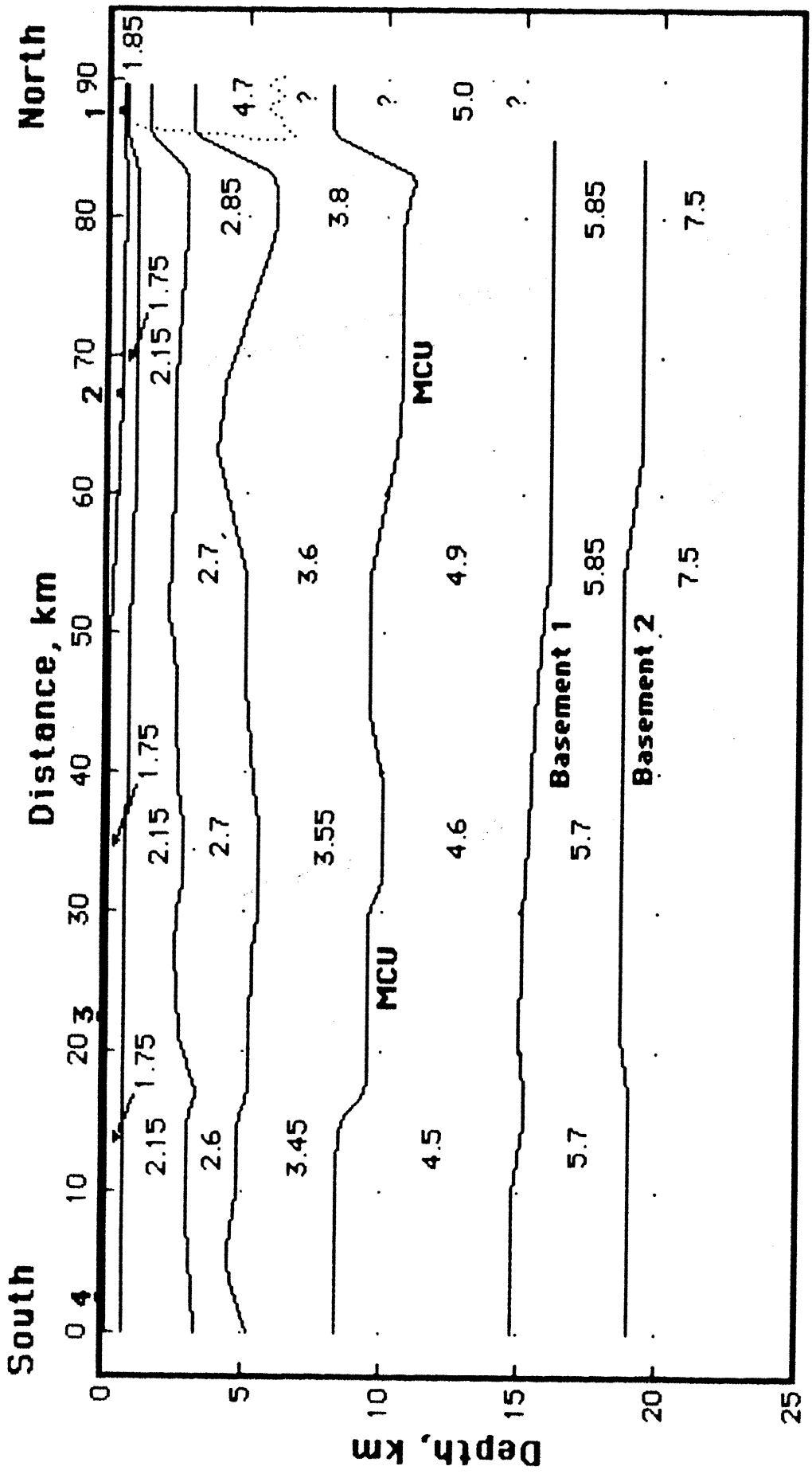

Fig. 9. Line 10 structural profile.

anticlinal structure at depth, a rim syncline, and the salt pillar. Reflections in the rim syncline are generally continuous with some high-amplitude arrivals. The structural high is landward of the rim syncline and its acoustic character is poorly resolved.

The data from the shallow section on OBS's 2, 3 and 4 contain a few well-defined reflections and strong, well-resolved refraction envelopes. At depth, each OBS has a suite of high-amplitude reflections from a surface we correlate with a middle Cretaceous unconformity. This horizon represents a prominent seismic arrival across the entire deep basin. I have also interpreted two deeper horizons, the first presumably the top of basement and the second an intracrustal surface. These are indicated in the data record by both wide-angle reflections and refractions with appropriate phase velocities and arrival times. No mantle phase velocities are indicated for a depth of at least 25 km.

OBS 1 was positioned on the crest of an interesting structure: 1) salt or high-velocity cap rock is fairly shallow in section, about 250 m below water bottom; 2) the column seems to consist of at least a double layer of salt. There is little confidence, however, in the interpretation of deeper structure from this OBS.

Overall, the upper sedimentary section probably consists of thick deep-marine shales sourced in the Rio Grande drainage basin. It is best considered part of the Tertiary Rio Grande Embayment depocenter. The entire sedimentary column is 15 to 16 km thick. There is some topographic relief in the MCU and this may be due to mobilized, non-diapiric salt. The top of basement dips gently northward, and little or no dip can be resolved on the intra-basement surface.
(F.J.S.)

Regional Interpretation and Discussion

The five seismic lines of this study covered an area roughly 2° x 2° in extent at the northwestern corner of the Gulf of Mexico, from the mid-shelf, across the slope and down to the continental rise. Although each line was interpreted more-or-less independently of the others by an individual, certain consistent structural patterns for the entire region emerge when one examines the above line interpretations as a suite.

The entire study area is covered with thick sediments, generally considered to be of Late Jurassic through Cenozoic age. The thickness of the sedimentary column is mostly between 13 and 15 km under the shelf and slope regions, but thins to about 11 km under the continental rise. Several velocity discontinuities, revealed by both near-vertical and wide-angle reflections, can be identified within the sedimentary column. The most prominent reflector, which is observed under all of the lines and which we interpret as the middle Cretaceous unconformity, is at a depth ranging from 7 to 11 km. This depth range includes 2 to 3 km of local relief found under most of the lines, interpreted to be caused by migration of salt that was deposited earlier.

The seismic P velocity at the top of the sedimentary column is 1.7 to 1.9 km/s, which is only slightly above the water-wave velocity and represents uncosolidated sediments. The velocity increases to 3.0 to 4.0 km/s just above the MCU, the lower value generally at shallower depth and higher value at deeper depth. The velocity range delineates mostly clastic material for this part of the column. Below the MCU, the velocity increases to 3.7 to 4.7 km/s, probably representing carbonate rocks or possibly some salt.

Various types of salt features are found in the sedimentary column. They range from small, diapiric bodies under Line 7 and larger diapirs of Lines 9 and 10 to allochthonous salt masses of Lines 8 and 9. Some of the anticlinal features of the MCU, such as those of Line 8, may be underlain by mobilized salt, although salt at this depth is indistinguishable from carbonate or other consolidated sediments by compressional-wave velocities alone.

A seismic velocity increase interpreted to be the top of the crust (basement) is observed under all lines at a fairly consistent depth of 13 to 16 km. The slight basement relief, however, is correlatable from line to line as seen in Fig. 10. A broad, depressed basement is observed trending NW-SE from the north end of Line 10 through the middle of Line 9 to the west end of Line 8. In contrast, a relatively uplifted basement is correlated from the northeastern half of Line 6 to the southwestern end of Line 7. This basement high may signify a seaward extension of the San Marcos Arch.

It should be noted that the boundary we identify as the basement, or the top of the crust, is derived mostly from seismic refraction arrivals and some wide-angle reflections. No near-vertical reflections clearly identified to be from this interface are observed on any of the OBS's. Since refracted rays transmit along minimum-time paths, it is quite likely that the major segments of refracted arrivals sample a layer at a depth somewhat below the top of the layer, where reflections may take place. This is especially true when there is an appreciable velocity gradient near the top of the layer. Therefore, the basement as identified in this study may be located deeper than the acoustic basement as recognized on multichannel seismic reflection data.

The observed seismic P velocity of the basement, at the top of the crust, ranges from 5.0 km/s to 6.4 km/s. The lower velocities, 5.0-5.2 km/s, are found in the northern half of the region under Lines 6 and 7, while the highest velocity, 6.4 km/s, is found under Line 8 at the southeastern corner of the region. Lines 9 and 10 show intermediate velocities in the range of 5.6 to 5.8 km/s. This clear trend in velocity variation may indicate a transition from continental crust under Lines 6 and 7 to an oceanic crust under Line 8, with intermediate transitional crust under Lines 9 and 10.

The Moho is observed only under Line 8, where it is located at a depth of 20 km below the continental rise, and appears to deepen towards the continental slope. The highest velocities observed at other lines range from 6.9 to 7.5 km at depths of 20 to 25 km. Thus, the Moho must be deeper than about 25 km under these lines.

The geologic interpretation of this area is common to that of other passive continental margins. Initial basin formation events most probably included crustal extension, subsidence, and the transition of sediment deposition from non-marine to abyssal oceanic facies. This initial stage is represented by the sediment interval between the basement and the MCU (UTIG Challenger Unit). Late Jurassic through Early Cretaceous in age, this unit is expected to consist of continental clastics, a thick section of evaporites, and shallow-to-deep marine clastics and carbonates. These latter facies would be hemipelagics, pelagics, and calcareous detritus, the downslope equivalent of the Lower Cretaceous reef systems. The thickness of this unit ranges from 7 km under the shelf to 3.5 km basinward. Allowing for salt migration, the original maximum thickness was probably about 5 km, including perhaps 2 km of salt. According to best estimates, the thickness of sediments of similar age underlying the present coastal regions may be the same or slightly less. We can thus speculate that we are defining a Late Jurassic - Lower Cretaceous depocenter. Further, while the overall sedimentation rate was low (compared to Gulf standards) we should expect sporadic

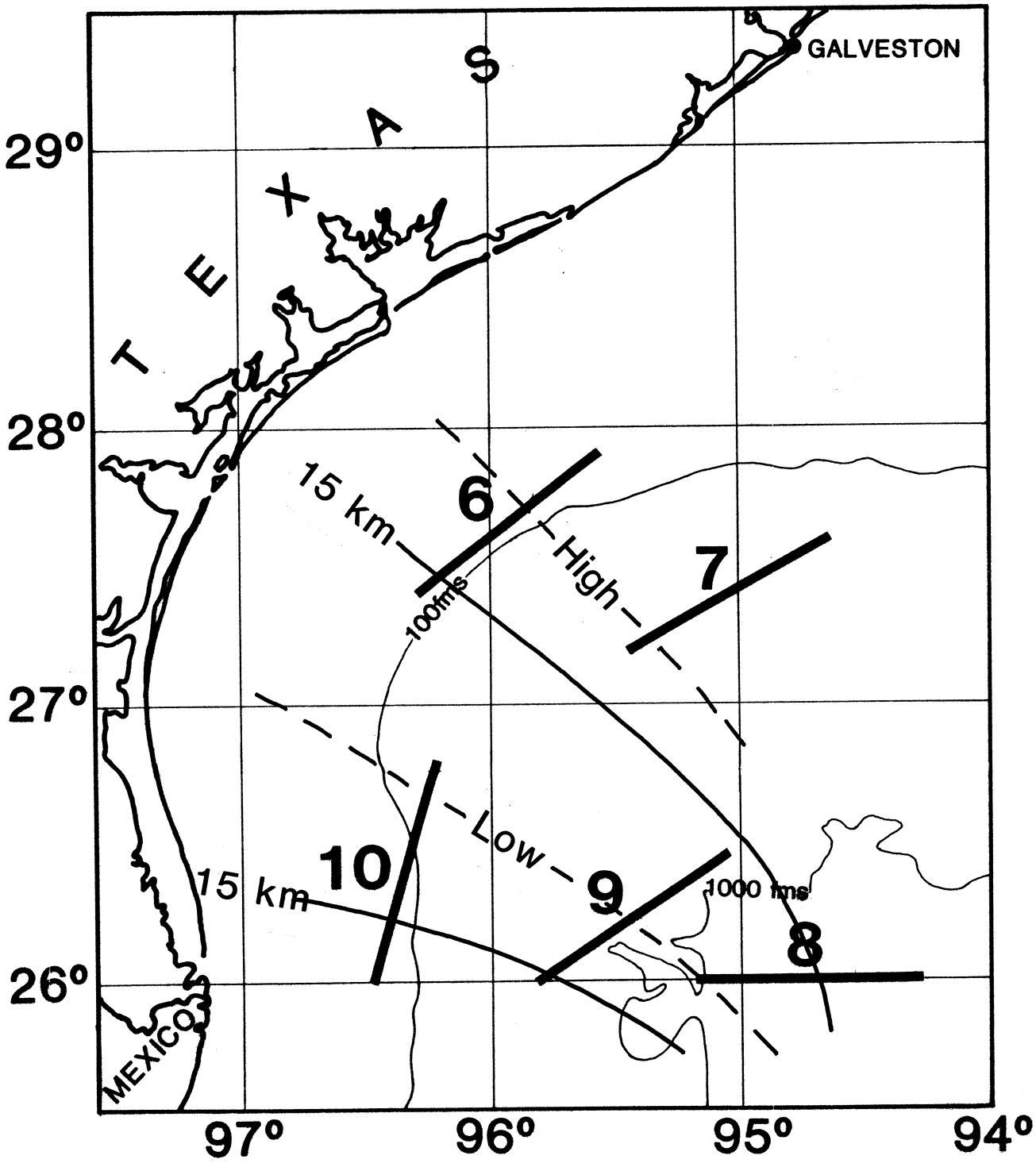

Fig. 10. Contour map showing the depth to the top of the basement.

episodes of turbidite deposition here or even the establishment of minor submarine fans.

As with many small ocean basins near continents, this early Gulf transgressive sedimentary regime was eventually succeeded by a regressive depositional environment. This transition in the Gulf was the result of two events: the Late Cretaceous - Tertiary orogenic episodes and the overall Tertiary sea level drop. Both served to rejuvenate drainage systems and vast quantities of clastics prograded basinward. A major delivery system was probably focused in the Rio Grande Embayment. Also canyons were incised into the linear Cretaceous reef and carbonate shoal margins of south Texas. A series of submarine fans was established under the present Texas coast and then overlain by massive progradational deltaic systems. Consequently 7.5-10 km of relatively unsorted clastic deposits accumulated downslope within our study area. The internal features of this thick sedimentary load include regional growth fault systems and undercompacted shale swells. These interact with the underlying evaporites to produce the present sediment-deformational continental margin.

Recommendations for Future Experiments

After this experiment was completed, it was clear that though the experiment was generally successful in revealing many structural features, there also were certain shortcomings. The following list of recommended solutions with discussion, which appeared in our first report (see footnote, page 1), still apply and therefore are repeated here with some updates.

1. Low signal level: Using air guns for seismic signal sources has clear advantages over using explosives in terms of uniformity of source signatures, high spatial density of shot points and high accuracy of shot times. However, the signal level of individual air-gun shots is low compared with those of explosives. This is a clear limitation especially when one desires to record deep refractions through a thick, poorly consolidated sedimentary section similar to what we encountered in this study area. Besides the obvious solution of increasing the capacity of air guns, which is not always feasible technically or economically, there are many ways to improve the observed signal level from air-gun shots.

a) Finding optimum air-gun depth: -- We used 2000 cubic inch air guns towed at a depth of 35 feet for this experiment. This was not only because we normally tow them at this depth for our multichannel work, but also because the bubble-pulse frequency at this depth of towing (about 6 Hz) is near the low end of the instrumental pass band, which is limited by our use of 4.5 Hz geophones. Although low frequency is advantageous for a long-distance transmission of seismic signals, it does not effectively utilize the surface ghost to enhance the emitted signal. Increasing the towing depth is expected to increase the bubble frequency and signal enhancement by ghost, but it also increases transmission loss. However, we have not conducted any controlled experiment to study these effects on signal reception at large distances. We recommend that such experiment be done to determine the optimum depth of towing of such air guns for wide-offset experiments.

b) OBS location: -- This study has revealed that signal strength of deep refractions is highly dependent on the bottom topography and near-surface geology. Deep refractions are generally strong when the shooting ship is over a basin or a region of well-stratified layers, but are very weak over complex salt structures. The

cause of this difference may be attributable either to focusing and defocusing of seismic rays by structures or to the difference in absorption and scattering of seismic energy through different geologic structures. Whatever the reason for this difference, we will be better off locating OBS's in basins or over well-stratified structures rather than over complex salt structures whenever possible.

c) Repeated shots: -- Detection of weak seismic signals at far distances is often accomplished by correlation of arrivals across several neighboring traces. Thus, theoretically the higher the spatial density of the sources, the better the chance of detecting weak signals because of the increased effective signal-to-noise ratio. For the present experiment, we shot far-offset portions of each line at 2.3 times higher spatial density than the rest. The result appears to be favorable, but not obvious. Perhaps we need a larger difference in spatial density to see the effect clearly. An extreme case will be to keep the shooting ship stationary while shooting a large number of shots at a given distance. However, we are not ready to recommend this except for experimental purposes because the additional ship time required to achieve appreciable improvement in the signal-to-noise ratio is quite significant and may even be uneconomical.

d) Multiple OBS's at one location: -- The other way to increase the data density for a better signal-to-noise ratio is to deploy more than one OBS at a given location. Assuming that they are separated by a distance sufficient to have independent background noise but close enough to detect essentially the same distant arrivals, we should be able to achieve significant improvement in signal-to-noise ratio. We had a chance to test this when we deployed two OBS's, OBS 5 and 6, within 100 m of each other during the reshoot of Line 7. The result is encouraging, especially because the availability of independent record sections from two OBS's allows us to confirm weak, uncertain arrivals on one record section with the other.

e) Geophone selection: -- We have not yet conducted any controlled experiment to determine the relative contributions of various possible sources of noise to the overall background noise. However, if the noise generated at the geophone and the input amplifier is significant, and we have a reason to suspect it may be, selection of geophones with higher output and larger suspended mass may improve the overall signal-to-noise ratio. The test 3-component OBS we deployed during this study contained geophones which were about 1/3 as sensitive as and less than 1/3 in suspended mass of our standard vertical-component geophones. The data taken with these 3-component geophones turned out to be significantly inferior to the others, proving our suspicion.

f) Background seismic noise: -- Background seismic noise plays a major roll in determining the overall signal-to-noise ratio of the data. We encountered two types of highly interfering background seismic noise during this study: wave noise and air-gun shots by other ships. Wave noise is particularly severe at shallow seas, but can be controlled by selecting relatively calm days to conduct the experiment. Other shooting ships can also be avoided by conducting the experiment during the period when other geophysical exploration ships are not expected in the area.

2. Line geometry: Unless the structure is nearly flat in all directions, the orientation of the shooting line and OBS locations are very important in acquiring readily interpretable data. In general, data from lines parallel to the strike of stratigraphic units are easier to interpret than those perpendicular to the strike, which may contain layers with rapidly changing depths. In areas of large lateral heterogeneities, reflections and refractions from features off the shooting line may significantly

influence the observation. Fortunately, since each OBS is completely detached from the shooting ship, there is no problem in deploying some OBS's off the shooting line. Off-line OBS's will help remove ambiguities of interpretation due to structural variations perpendicular to the shooting line. If appropriate, non-linear shooting geometry may also be adopted to further enhance the lateral control. For future experiments, it is recommended that due consideration be given to the most appropriate geometry for shooting lines and OBS locations.

3. Data analysis techniques: Though we have found it most successful to use 2-D ray tracing in dealing with complex structures like those found in this study area, the technique is non-unique, and the resulting structure may not be a correct one. One way to test the validity of the derived structure is to compare synthetic seismograms based on the derived model to the observations. Therefore, we recommend that such an approach be developed for use in future studies.

Conclusions

1. The northwestern Gulf of Mexico, offshore of Texas, is covered with thick sediments 13 to 15 km thick under the shelf and slope and 11 km thick under the continental rise.

2. Several seismic reflectors are found within the sedimentary column, the most prominent of which is at a depth of 7 to 11 km, which we identify to be the middle Cretaceous unconformity (MCU). This discontinuity shows 2 to 3 km relief, possibly caused by mobilized salt.

3. The seismic P velocity in the sedimentary column above the MCU increases from 1.7-1.9 km/s near the sea floor to 3.0-4.0 km/s just above the MCU. This velocity range is appropriate for clastic sediments.

4. Below the MCU, the sedimentary velocity increases to 3.7-4.7 km/s, probably representing carbonate rocks or possibly some salt.

5. Several types of salt features are found in the sedimentary column, ranging from small diapiric bodies and large diapirs to allochthonous salt masses.

6. The basement (top of the crust) is found at a depth of 13 to 16 km. Its relief is quite consistent from line to line and shows a NW-SE trending trough and also a NW-SE trending uplift that may represent a seaward extension of the San Marcos Arch.

7. The seismic P velocity in the upper crust shows a clear trend from the northern (5.0-5.2 km/s) to the southern (5.6-5.8 km/s) part of the study area and then to the continental rise (6.4 km/s), indicating a transition from mostly continental to transitional and then to oceanic crust.

8. The Moho is observed at a depth of 20 km under the continental rise, and appears to deepen towards the continental slope; but under most of the slope and shelf, it was not observed, suggesting it to be deeper than about 25 km.

Acknowledgements. The ocean-bottom seismographs used for the experiment were designed principally by Paul L. Donoho, now with Chevron Oilfield Research Co., working under the direction of Gary V. Latham, now with Cities Service. Phillip H.

Roper, Paul M. McPherson and Michael Butterfield were responsible for building, maintenance and operation of the instruments as well as many other related mechanical, electronic and programming tasks. Captain Bruce H. Collins of R/V *Fred H. Moore* and his crew were extremely helpful in making this experiment successful. Kenneth H. Griffiths, Dale S. Sawyer, Susan Walker, George W. Pearcy, Oscar Febres-Cordero and Christopher Bennett were responsible for many ship-related operations including electronics, mechanical work, navigation, data acquisition and communications. William P. O'Brien, Jr. assisted with OBS operations, and Joseph O. Ebeniro was of utmost help in processing the acquired data on board.